



In-situ scattering study of a liquid-liquid phase transition in Fe-B-Nb-Y supercooled liquids and its correlation with glass-forming ability

Jiacheng Ge^a, Haiyan He^b, Jing Zhou^c, Chenyu Lu^b, Weixia Dong^a, Sinan Liu^a, Si Lan^{a,b,*}, Zhenduo Wu^b, Anding Wang^d, Liang Wang^e, Cun Yu^f, Baolong Shen^{c,**}, Xun-li Wang^{b,g,***}

^a Herbert Gleiter Institute of Nanoscience, School of Materials Science and Engineering, Nanjing University of Science and Technology, 200 Xiaolingwei Avenue, Nanjing, China

^b Department of Physics, City University of Hong Kong, 83 Tat Chee Avenue, Kowloon, Hong Kong, China

^c School of Materials Science and Engineering, Southeast University, Nanjing 211189, Jiangsu, China

^d Department of Materials Science and Engineering, City University of Hong Kong, 83 Tat Chee Avenue, Kowloon, Hong Kong, China

^e School of Materials Science and Engineering, Beijing Institute of Technology, Beijing 100081, China

^f Zwick China Ltd., Unit 1022, No. 999 Wangqiao Road, Chuansha Pudong District, Shanghai 201201, China

^g Center for Neutron Scattering, City University of Hong Kong Shenzhen Research Institute, 8 Yuexing 1st Road, Shenzhen Hi-Tech Industrial Park, Nanshan District, Shenzhen, 518057, China

ARTICLE INFO

Article history:

Received 28 December 2018

Received in revised form

8 February 2019

Accepted 9 February 2019

Available online 11 February 2019

Keywords:

Bulk metallic glasses

Liquid-liquid phase transition

Crystallization

Locally favored structures

Glass-forming ability

ABSTRACT

In-situ synchrotron high-energy X-ray diffraction was used to study the kinetics of structure evolution for two Fe-based bulk metallic glasses with different thermophysical behaviors upon heating and isothermal annealing in the supercooled liquid region. It is found that the structure change of $(\text{Fe}_{0.72}\text{B}_{0.24}\text{Nb}_{0.04})_{97}\text{Y}_3$, an average glass former, follows a continuous disordering process before crystallization, while that of $(\text{Fe}_{0.72}\text{B}_{0.24}\text{Nb}_{0.04})_{95.5}\text{Y}_{4.5}$, a better glass former with an anomalous exothermic peak below the crystallization temperature, is characterized by a reentrant supercooled liquid behavior. A hidden amorphous phase with a configurationally highly-correlated structure is found at a critical temperature of the anomalous exothermic peak for the $(\text{Fe}_{0.72}\text{B}_{0.24}\text{Nb}_{0.04})_{95.5}\text{Y}_{4.5}$ supercooled liquid, and then it reenters the disordered phase of lower correlation length at a higher temperature. Synchrotron diffraction and the density measurements together illustrate that the liquid-liquid phase transition accompanies with an unusual density change upon isothermal annealing at the anomalous exothermic peak temperature. Our experimental results suggest that a liquid-liquid phase transition which occurred at the medium-range length scale plays an important role in stabilizing the $(\text{Fe}_{0.72}\text{B}_{0.24}\text{Nb}_{0.04})_{95.5}\text{Y}_{4.5}$ supercooled liquid. Possible mechanisms for the observed differences and the relationship with the glass-forming ability are discussed based on the results of the pair distribution function analysis.

© 2019 Elsevier B.V. All rights reserved.

1. Introduction

Liquids/glasses, like their crystalline counterparts, can have polymorphs. Liquid-liquid phase transition (LLPT) means that the

liquids with the same composition but different locally favored structures (LFSs) can transform to each other upon cooling/heating [1]. LLPT has been found to be a universal phenomenon [2,3]. However, the origin of LLPT remains elusive and even controversial. The cooperative arrangement of bond-orientation orders, that is, LFSs, upon cooling/heating has been proposed to be responsible for the LLPT in molecular liquids such as water [4] and triphenyl phosphite (TPP) [5]. The LLPT in atomic liquids was suggested to occur at high temperature [6] and pressure [7]. Recently, a hidden LLPT was revealed in Pd-Ni-P bulk metallic glasses (BMGs) accompanied by an anomalous exothermic peak (AEP) upon heating [8]. The AEP was identified to be located in the supercooled

* Corresponding author. Herbert Gleiter Institute of Nanoscience, School of Materials Science and Engineering, Nanjing University of Science and Technology, 200 Xiaolingwei Avenue, Nanjing, China.

** Corresponding author.

*** Corresponding author. Department of Physics, City University of Hong Kong, 83 Tat Chee Avenue, Kowloon, Hong Kong, China.

E-mail addresses: lansi@njust.edu.cn (S. Lan), blshen@seu.edu.cn (B. Shen), xlwang@cityu.edu.hk (X.-l. Wang).

liquid region, which is just above the glass transition temperature T_g and far below the crystallization temperature T_x .

It has been found that the AEP also exists in a variety of BMGs, including Zr-based [9–13], Fe-based [14], Mg-based [15], and Ni-based alloys [16], etc. The AEP in BMGs attracted much attention because it opens a window to build up a correlation between the hidden phase transitions and glass-forming ability (GFA). For example, Fe-B-Nb-Y BMGs with an AEP has good soft magnetic property (e.g., low coercivity) and excellent GFA [14]. Studies have been done, mostly by ex-situ characterizations, to investigate the structure change at short-range order (SRO) [17]. However, more and more evidence indicated that the structure change beyond the short-range length scale plays a more critical role in phase transitions, including LLPT [8,18], crystallization [9,19], etc. Therefore it is desirable to in-situ study the hidden LLPT and probe the structural evolution at multiple length scales, from short-range to medium-range and nanoscale, for the Fe-based BMGs in the temperature region of the AEP.

In this paper, the experimental evidence was obtained for the hidden LLPT which occurred in the same temperature region of AEP in the supercooled liquid region of a Fe-Nb-Y-B BMG using in-situ synchrotron high-energy X-ray diffraction (HE-XRD), small-angle X-ray scattering (SAXS) as well as differential scanning calorimetry (DSC). For easy presentation, the studied alloys, $(\text{Fe}_{0.72}\text{B}_{0.24}\text{Nb}_{0.04})_{97}\text{Y}_3$ and $(\text{Fe}_{0.72}\text{B}_{0.24}\text{Nb}_{0.04})_{95.5}\text{Y}_{4.5}$, were abbreviated as Y3 and Y4.5. The Y4.5 alloy exhibits an AEP while Y3 does not. Chemical phase separation at nanoscale and crystallization were ruled out in the AEP temperature region of Y4.5. It turns out that the supercooled liquid achieves an ordered state first and then reenters into a more disordered state at a higher temperature above the AEP upon heating. The synchrotron diffraction and density measurements demonstrate that the density of Y4.5 alloy decreases after the LLPT when annealing in the AEP temperature region. The atomic scale structure change at medium-range length scale is found to play an important role during LLPT. Furthermore, it is suggested that the stabilization of the supercooled liquid in the AEP alloy, Y4.5, is correlated with the improved GFA.

2. Experimental

2.1. Sample preparation

Fe (99.9%), B (99.5%), and Nb (99.9%) elements were carefully weighed in the right proportion and were melted by induction to obtain the ingots of $\text{Fe}_{72}\text{B}_{24}\text{Nb}_4$. Then Y (99.9%) were weighed and added to the ingots by arc melting. Before suction cast, the surface oxide layer on the ingot was removed with a grinder to prevent heterogeneous nucleation. Finally, glassy rods of $(\text{Fe}_{0.72}\text{B}_{0.24}\text{Nb}_{0.04})_{97}\text{Y}_3$ and $(\text{Fe}_{0.72}\text{B}_{0.24}\text{Nb}_{0.04})_{95.5}\text{Y}_{4.5}$, which are abbreviated as Y3 and Y4.5 respectively, with diameter ~ 2 mm and length ~ 70 mm were prepared by suction cast method. Ribbons were prepared by melt-spinning. The DSC curves were measured using platinum crucibles with Netzsch DSC 404 F3 in a high-purity Ar atmosphere with a scanning rate of 20 K min^{-1} .

2.2. Characterization

Synchrotron HE-XRD for pair distribution function (PDF) analysis were conducted at beamline 11-ID-C at the Advanced Photon Source, Argonne National Laboratory. High energy x-rays with a beam size of $500 \mu\text{m} \times 500 \mu\text{m}$ and wavelength of 0.1173 \AA were used in transmission geometry for data collection. Two-dimensional (2D) diffraction patterns were obtained using a Perkin Elmer amorphous silicon detector. The data acquisition time for each pattern was 1 s. The time for data readout and saving was ~ 4 s.

The heating rate was 20 K min^{-1} . So the time resolution was around 5 s and the temperature resolution was 1–2 K. The static structure factor, $S(Q)$ with $Q_{\text{max}} \sim 30 \text{ \AA}^{-1}$, was derived from the scattering data after masking bad pixels, integrating images, subtracting the appropriate background and correcting for oblique incidence, absorption, multiple scattering, fluorescence, Compton scattering, and Laue correction using Fit2D and PDFgetX2. The reduced pair distribution function (PDF), $G(r)$, is obtained from the Fourier transform of $S(Q)$, $G(r) = (2/\pi) \times \int_0^{Q_{\text{max}}} Q(S(Q) - 1) \sin(Qr) dQ$, where r is the distance in real space and $Q = 4\pi \sin\theta/\lambda$. Here θ is half of the scattering angle between the incident beam and the scattered beam. λ is the X-ray wavelength.

SAXS measurements were conducted on the SAXSpace line collimation camera. All samples were cut and thinned to be foils with 30–40 μm thickness to ensure the appropriate transmittance. The sample chamber was evacuated to a vacuum of 10^{-3} torr to reduce the background noise. The scattering patterns were acquired in a transmission geometry using a 2D detector. The 2D images were integrated azimuthally, corrected for background scattering and normalized using SAXStreat and SAXSquant software (Anton Paar). Density measurement was conducted using a METTER TOLEDO Instructions XP Analytical Balance based on the Archimedes' principle. The N-Hexadecane-D34 solution was employed during the density measurement. The mass density of Y4.5 alloys before and after treatment was measured repeatedly at least 5 times to reduce the measuring error.

3. Results

3.1. Thermo-physical behavior, AEP, and GFA indicators

Fig. 1 shows the DSC measurement results and the HE-XRD diffraction patterns for Y3 and Y4.5 BMGs. Fig. 1(a) is the scanning curves for Y3 (blue) and Y4.5 (red) BMGs. Thermophysical parameters have been summarized in Table 1. In Y4.5, there is an AEP above the T_g . The valley of the AEP, T_C , is ~ 908 K. The T_g for Y4.5 is ~ 12 K higher than that of the T_g of Y3, indicating a more stable glassy state for the AEP BMG. The T_{X1} of Y4.5 is ~ 34 K higher than that of Y3. Therefore, the range of the supercooled liquid region of Y4.5 is ~ 22 K wider than that of Y3, indicating more stable supercooled liquid for Y4.5 alloys.

The calculated GFA indicators for Y4.5, including the reduced glass transition temperature T_{rg} and Gamma value γ , are larger than those of Y3, which is consistent with the critical casting thickness as shown in Table 1. There is no detectable difference between the DSC curve of the rods and that of ribbons of Y4.5 alloys from Fig. 1(b). Furthermore, the AEP for Y4.5 BMGs disappeared after annealing at T_C with a period of ~ 300 s. The T_g for Y4.5 shifts to ~ 878 K, which is ~ 21 K higher than that of the as-cast Y4.5 BMG and ~ 33 K higher than that of the as-cast Y3 BMG, suggesting that the Y4.5 achieves a much more stable glassy state after annealing.

3.2. In-situ synchrotron X-ray diffraction study of liquid-liquid phase transition

To gain physical insights into the DSC results, as shown in Fig. 1(c) and (d), in-situ synchrotron HE-XRD measurements were carried out for Y4.5 and Y3 upon heating. The diffraction pattern at $\sim T_C$ shows that the sample is still in the amorphous state. The Rietveld refinement results in Fig. 2(a) and (b) illustrate that the crystalline phase for Y4.5 (B_6Fe_{23} , space group: $Fm-3m$) is less ordered than those of Y3 (B_6Fe_{23} , space group: $Fm-3m$ and BFe_2 , space group: $I4/mcm$) after heating to ~ 1003 K. The HE-XRD results thus confirm that the Y4.5 supercooled liquids are more stable to resist crystallization, which is consistent with the better GFA of Y4.5.

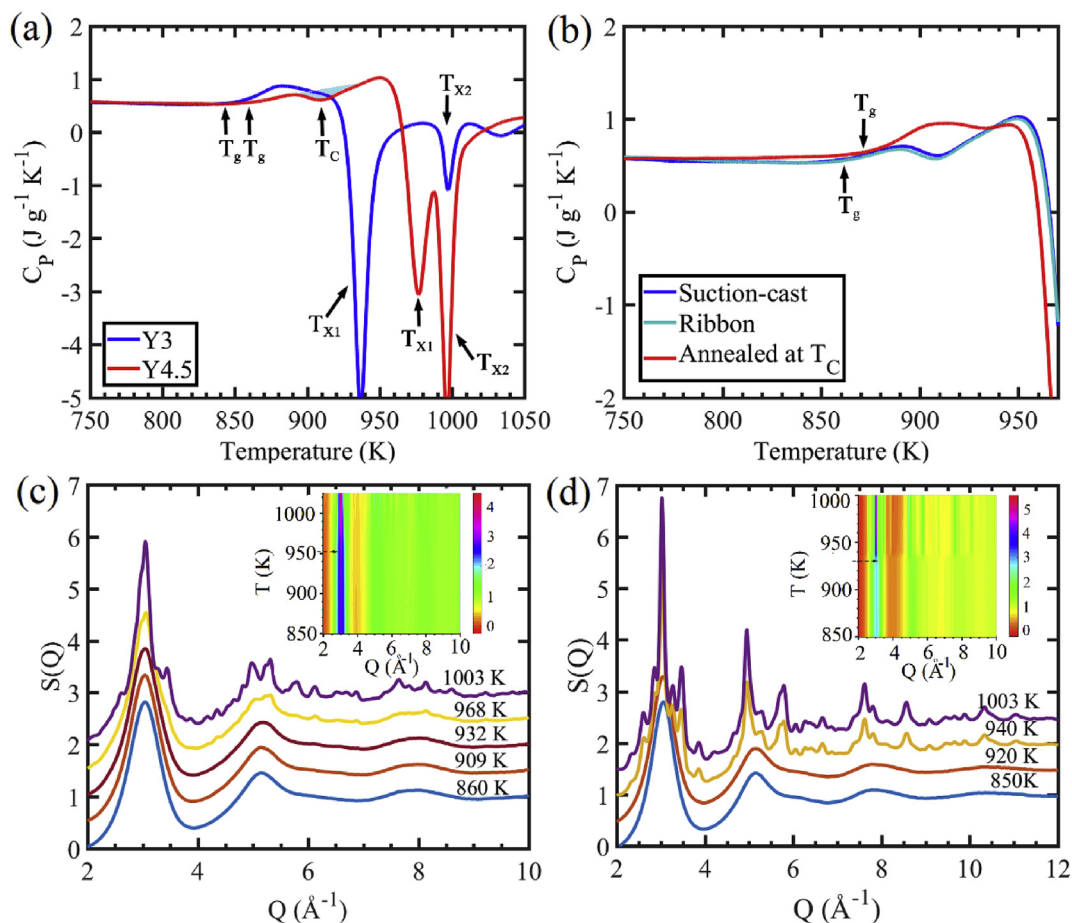


Fig. 1. Thermal scanning of (a) the Y4.5 and Y3 BMGs in as-cast state and (b) for Y4.5 BMGs with different thermal history. The heating rate was 20 K min^{-1} . The structure factor, $S(Q)$, at different temperature upon heating above the crystallization temperature for (c) Y4.5 alloys and for (d) Y3 alloys. The 2D contour plots show the crystallization temperatures, T_x , revealed by in-situ synchrotron diffraction for both alloys, which are consistent with the thermal analysis results.

Table 1

Thermophysical parameters T_g , T_x , T_i , T_{rg} , γ , and critical thickness for Fe-B-Nb-Y BMGs.

Composition	T_g (K)	T_x (K)	T_c (K)	T_i (K)	T_{rg}	γ	D_c^a (mm)
(Fe _{0.72} B _{0.24} Nb _{0.04}) ₉₇ Y ₃	845	924, 988	—	1430 ^a	0.591	0.406	4
(Fe _{0.72} B _{0.24} Nb _{0.04}) _{95.5} Y _{4.5}	857	958, 988	908	1349 ^a	0.635	0.434	7

^a From Ref. [14].

Fig. 3 (a) and 3(b) show the structure factor, $S(Q)$, of Y4.5 and Y3 BMGs upon heating. Fig. 3(c) and (d) are their corresponding differential $S(Q)$, which was obtained by subtracting the diffraction pattern at a temperature close to the T_g . There is an unusual structure change as indicated by the dotted line for the first sharp diffraction peak (FSDP), Q_1 , of the $S(Q)$ for the Y4.5 BMG. The differential $S(Q)$ at 905 K, $\sim T_c$, shows an inconsistent profile with those patterns at temperatures above and below T_c . However, the differential $S(Q)$ evolves consistently for the Y3 BMG. Fig. 4 shows the SAXS profiles of Y4.5 at the as-cast state and after annealing at a temperature close to T_c with a period of about 300 s. The developing profiles as a function of Q are almost overlapping with each other, confirming that in the Y4.5 alloy after isothermal annealing there is no resolvable phase separation at the nanoscale (2–40 nm).

Further peak analysis for the FSDP, Q_1 , has been done to identify the anomalous structure change for Y4.5 AEP alloy. Fig. 5 shows the results of the first moment and the second moment analysis as a function of temperature, corresponding to the peak position and width respectively [18]. The analysis of moments was often used to

avoid the subjectivity of assumed functions for the peak shape of the asymmetric FSDP. Peak position and width of the FSDP were suggested to be linked to the density and correlation length for the glasses/liquids [20]. As shown in Fig. 5(b) and (d), the values of the first and second moments develop linearly above and below the glass transition for Y3 BMGs. However, in Fig. 5(a) and (c), the Q_1 value shows a slope change at T_c for Y4.5 BMGs. The anomalous structure change for Y4.5 suggesting a hidden LLPT occurred in association with the AEP at T_c . More interestingly, the second moment shows a discontinuous change at T_c . The Y4.5 supercooled liquid initially becomes more correlated and then goes back to a less correlated state at a high temperature after T_c , indicating the reentrant behavior of the supercooled liquid upon heating.

3.3. The real-space analysis and density measurements

To find out the atomic scale structure origin of the LLPT, Fig. 6(a) shows the reduced PDF $G(r)$, obtained by the Fourier transform of $Q(S(Q)-1)$. The first peak r_1 in $G(r)$ corresponds to the nearest

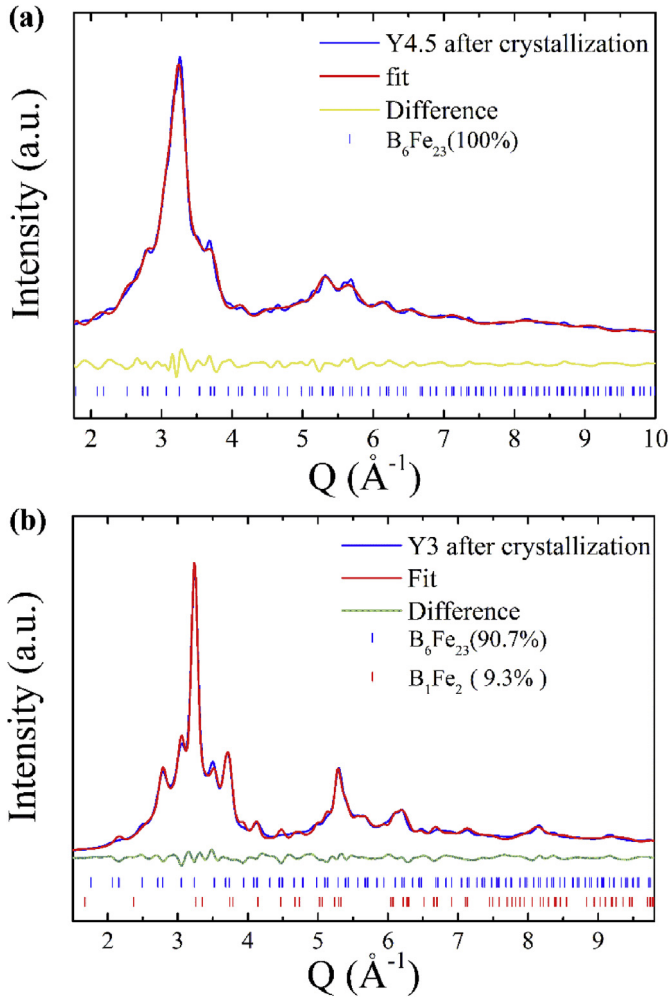


Fig. 2. Rietveld refinement results for (a) Y4.5 alloys and (b) Y3 alloys after crystallization, revealing the crystalline products for both alloys.

neighbor shell and can be used to identify the structure information of solute-centered SRO. The shoulder of the second peak, r_{22} , indicates the extended-range order beyond the nearest neighbor shell, that is, packing connectivity [21]. Fig. 6(c) shows the integrated intensity for r_1 (for the region $G(r) \geq 0$) and the integrated intensity for r_{22} (for the region 4.94–4.95 Å). For comparison, the Y-axis range of the plots was set at ± 9 –12%, and DSC profiles were also superimposed. As shown in Fig. 6(d), there is no anomalous structure change for Y3 BMGs. However, for Y4.5 AEP BMGs, the intensity change of r_1 shows a small change through the transition temperature. The most surprising feature is the intensity change of r_{22} , which shows a rise and fall in T_C , indicating the consistent structure change with the reentrant behavior in AEP alloys.

The slope change of the Q_1 as a function of temperature indicate that there is a thermal expansion anomaly at T_C due to the occurrence of possible LLPT. Therefore, synchrotron diffraction and density measurement are necessary to reveal the nature of LLPT further. Fig. 7(a) and (b) show the $S(Q)$ and the $G(r)$ patterns for a Y4.5 glass under isothermal annealing at the T_C temperature. The diffraction patterns at different temperature illustrate that, even after annealing 6000 s at T_C , the sample maintains at the amorphous state. Moreover, the shoulder peak r_{22} of the $G(r)$ patterns for Y4.5 after annealing a period at T_C is more pronounced than that of the initial state. Fig. 7(c) shows the results of the first moment and

the second moment analysis for the FSDP, Q_1 , as a function of isothermal time. Both the first moment and the second moment of Q_1 decrease during isothermal annealing and tend to be a plateau at the end (~ 6000 s), suggesting that the density decreases and the correlation length of the ordered structure increases. Besides, Fig. 7(d) shows the integrated intensity for r_1 and r_{22} in $G(r)$ patterns as a function of annealing time. The intensity of r_{22} rises while the intensity of r_1 does not change much during annealing. These changes further demonstrate that the cluster connectivity was enhanced after the LLPT. The correlation between the peak position and the mass density in BMGs was revealed before [20,22,23]. Density can be measured using the fluid displacement method based on the Archimedes' principle [24]. Fig. 8 shows the value change of $Q_1^{2,31}$ under isothermal annealing and the measured density change during the LLPT. The value of $Q_1^{2,31}$ is in the right proportion to the mass density, following the relationship, $Q_1 \cdot V_a^{0.433 \pm 0.007} = 9.3 \pm 0.2$ [20]. Moreover, the value of $Q_1^{2,31}$ decreases after annealing, and it is coincident with the change of the measured mass density.

4. Discussion

4.1. Effect of the change of the driving force on nucleation after LLPT and the correlation with GFA

Our results suggest a correlation between the AEP and GFA for the soft magnetic Fe-B-Nb-Y BMGs. The AEP in the supercooled liquid region has been studied in Fe-based MGs [14,17,25], but few works relate it with the GFA. The hidden LLPT, which could be brought out upon heating/annealing in the supercooled liquid region, connects the AEP and GFA for the Fe-B-Nb-Y supercooled metallic liquids. According to the glass transition theories [26–30], the cooperative rearrangement of LFSs, that is, short-to-medium range orders (SRO and MRO), would play an important role during the liquid-to-glass transition. Upon heating the Y4.5 to a temperature above T_g but below T_C , the supercooled liquid transforms from a phase of less correlation length to another phase of larger correlation length. Furthermore, when heating the Y4.5 above T_C but below T_X , the supercooled liquid, driven by entropy, goes back to the disordering phase with less correlation length at a higher temperature. The unusual growth in a correlation length of the LFSs has been revealed by simulations [31] and experiments [18,32–34] for the metallic glass-forming liquids. Presumably, the newly-formed liquid phase with highly-correlated LFSs in the vicinity of glass transition temperature has slower dynamics (that is, smaller diffusion coefficient or larger overall viscosity) [35] and plays a vital role in stabilizing the supercooled liquids.

The Y4.5 alloys quenched from the supercooled liquid after the occurrence of LLPT has more stable glassy and supercooled liquid states than those of Y3 alloys. There is no AEP for the Y4.5 BMG after annealed at $\sim T_C$. Furthermore, the annealed Y4.5 MGs show much higher T_g (~ 33 K) and broader supercooled liquid region than those of as-cast Y3 MG, which means the new amorphous phase has a lower energy state and might encounter a higher energy barrier during subsequent crystallization in the Y4.5 supercooled liquid after the occurrence of LLPT. The nucleation rate [36] is defined as a function of chemical potentials (Δg) and interfacial energy (σ) between the precipitates and the amorphous/liquid matrix:

$$I^{st} \propto D \cdot \exp(-W^*/k_B T) \quad (1)$$

where W^* is known as the nucleation barrier, which can be expressed as $W^* = 16\pi\sigma^3/3(\Delta g)^2$, and D is the diffusion coefficient. Δg is right proportional to the undercooling, $\Delta T = (T_1 - T)$. Y4.5 alloys have a lower T_1 than that of Y3 (Table 1). So for the same

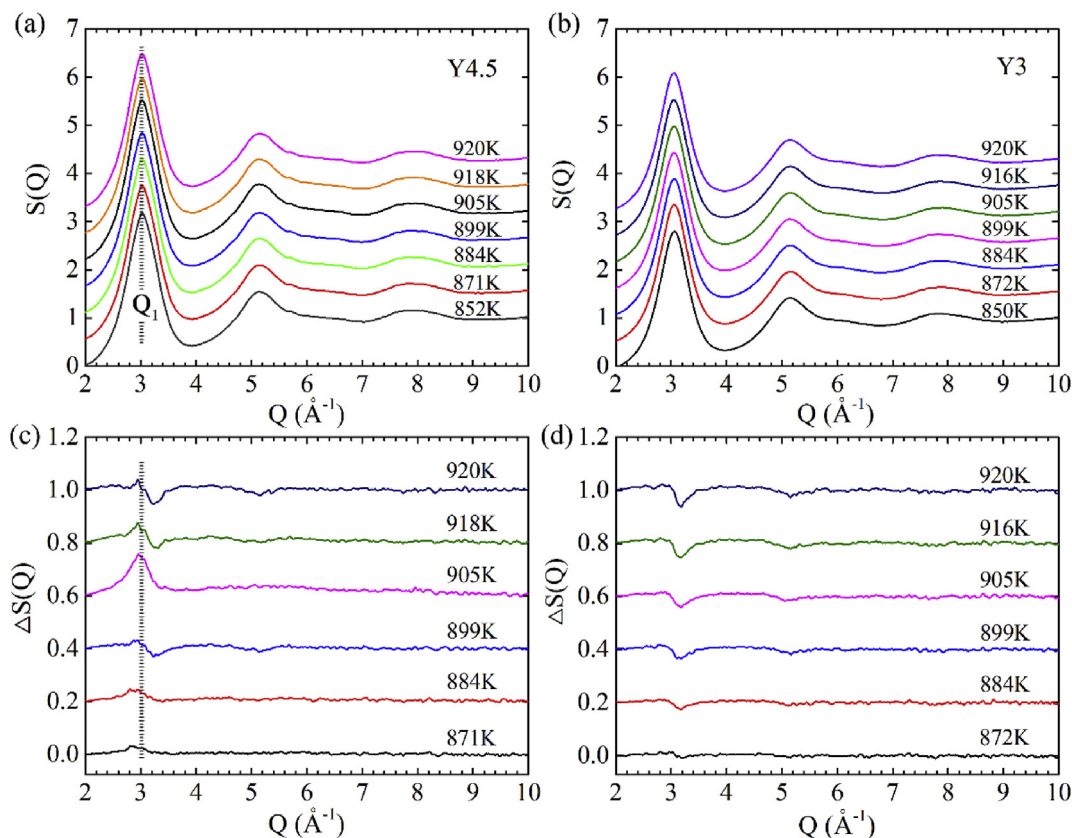


Fig. 3. In-situ high-energy synchrotron X-ray study of Y4.5 and Y3 metallic glasses upon heating. The $S(Q)$ patterns at different temperature (a) for Y4.5 alloys and (b) for Y3 alloys. Differential structure factor, $\Delta S(Q)$, at different temperature (c) for Y4.5 MGs and (d) for Y3 MGs. The heating rate was 20 K min^{-1} .

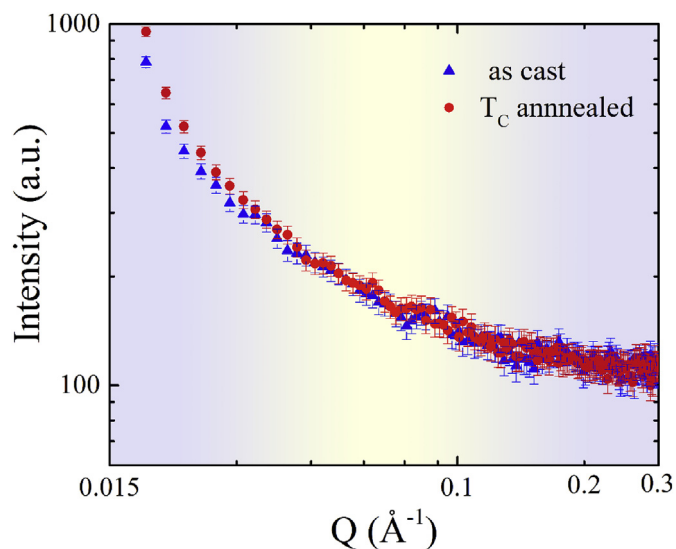


Fig. 4. The small angle X-ray scattering profiles for Y4.5 alloys in the as-cast state (blue triangles) and annealed state (red dots). The Y4.5 sample was annealed at T_c with a short period, $\sim 300 \text{ s}$. (For interpretation of the references to colour in this figure legend, the reader is referred to the Web version of this article.)

crystallization temperature, the ΔT of Y4.5 is smaller than that of Y3. Therefore, the Δg of Y4.5 would be smaller than that of Y3. After the occurrence of the LLPT, the newly-formed supercooled liquid has more correlated LFSs, that is, SRO and MRO. The local symmetry

of LFSs is usually different from the crystalline order [37–41]. Presumably, the presence of highly-correlated LFSs would raise the interfacial energy σ between the new liquid phase and the crystalline solid for Y4.5 supercooled liquid [27,35,42]. So the nucleation barrier for the Y4.5 supercooled liquid after the occurrence of LLPT would be larger than that of the Y3 supercooled liquid, which thus reduces the nucleation rate.

It was reported that the supercooled liquids of excellent GFA also correspond to a slow growth rate of the crystal embryos due to the ‘pinning’ effect [43] of LFSs. The atomic radius for Fe, Nb, B, Y is 0.126 nm, 0.146 nm, 0.086 nm, and 0.174 nm, respectively [14,44]. The Y element has the largest atomic size among all constituent elements and possesses the slowest mobility among all atoms [45–47]. On the other hand, the enthalpy of mixing for Y-B has a much negative value in the Fe-B-Nb-Y alloy systems, $\sim -50 \text{ kJ mol}^{-1}$, which would enable the formation of stable clusters of local ordering to frustrate the growth of crystal embryos [17]. Furthermore, although thermal stability does not necessarily correlate with GFA [48], stable glass-forming liquids with pronounced SRO and MRO, such as Y4.5 alloys, often have an excellent GFA.

4.2. The role of cluster connectivity on LLPT

Our experiment rules out the occurrence of crystallization or chemical phase separation at nanoscale when heating the Y4.5 BMG to the AEP temperature region. The HE-XRD can resolve nanocrystalline phases of a 10^{-6} vol fraction [18]. According to the in-situ XRD results (Fig. 3), there is no hint for the occurrence of crystallization at T_c . Although the heat of mixing between Y and Nb elements is $+30 \text{ kJ mol}^{-1}$, SAXS measurements in Fig. 4 reveal that

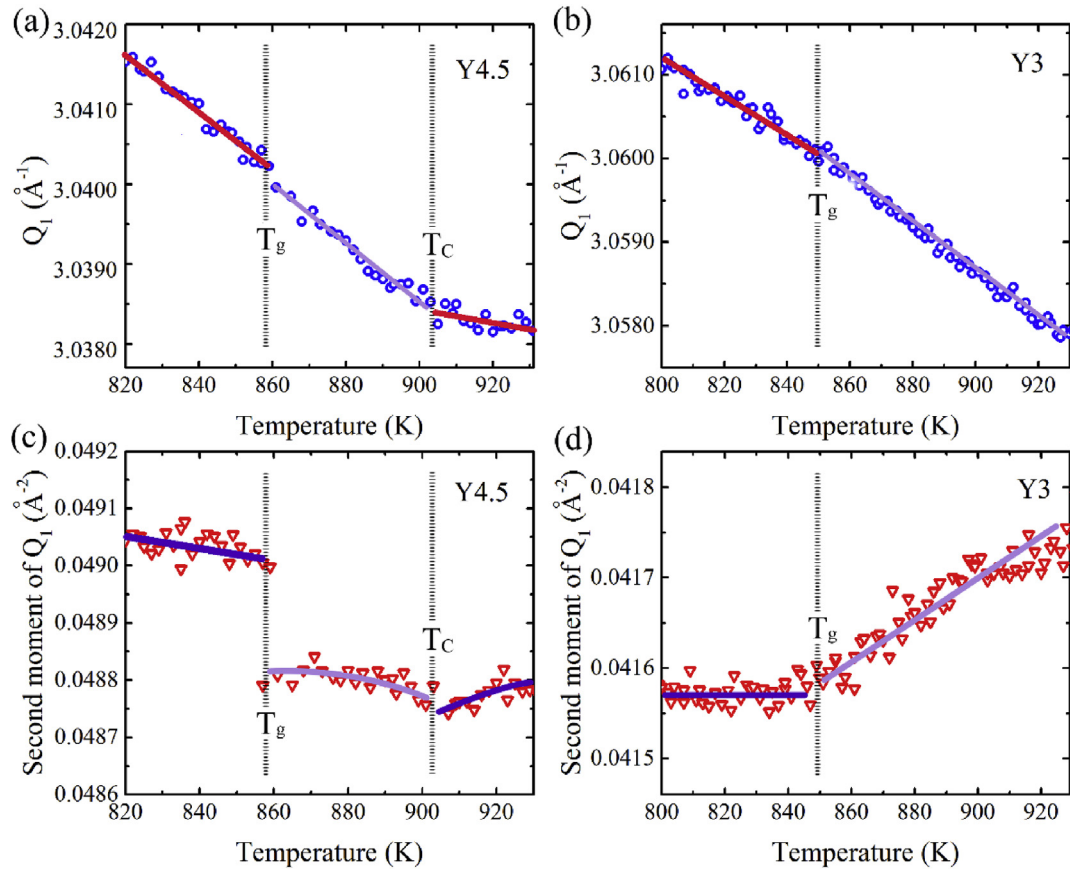


Fig. 5. Profile analysis results of the first sharp diffraction peak of $S(Q)$. The first moment changes as a function of temperature (a) for Y4.5 alloys and (b) for Y3 alloys. The second moment changes as a function of temperature (c) for Y4.5 alloys and (d) for Y3 alloys. The solid lines serve as a guide to the eyes.

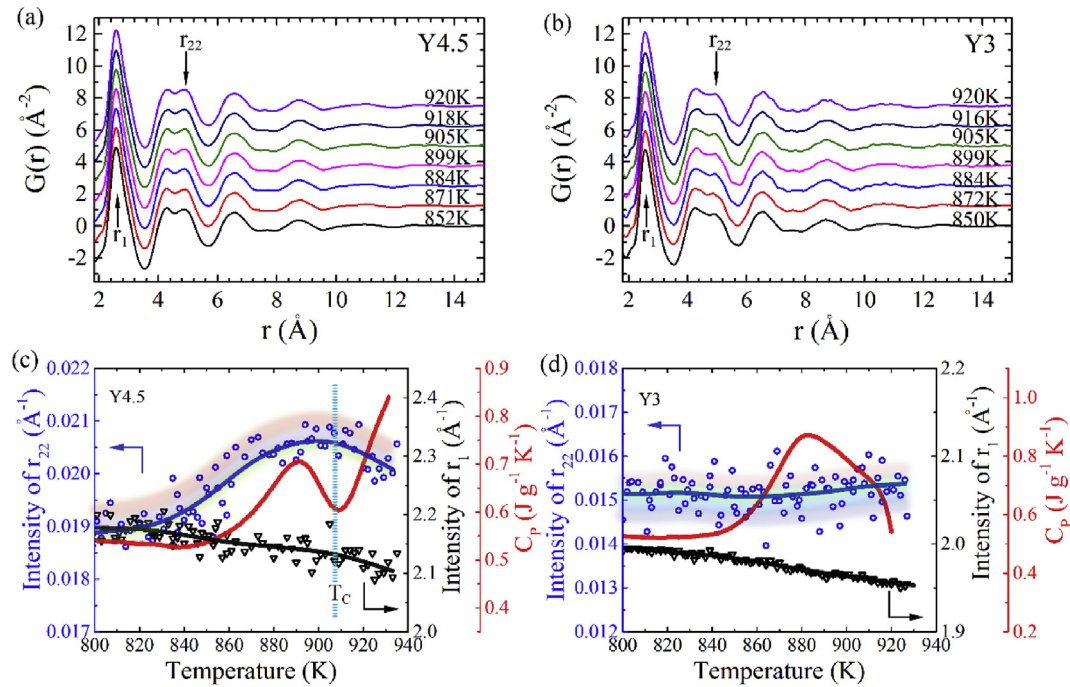


Fig. 6. Real-space analysis of the synchrotron diffraction results. The reduced pair distribution function, $G(r)$, at different temperature upon heating (a) for Y4.5 alloys and (b) for Y3 alloys. The intensity change of the first coordination shell, r_1 , and the shoulder of the second coordination shell, r_{22} , as a function of temperature (c) for Y4.5 alloys and (d) for Y3 alloys. The DSC curves have been superimposed for comparison. The solid lines are the results of a smooth spline fitting. The bands are guide to the eyes.

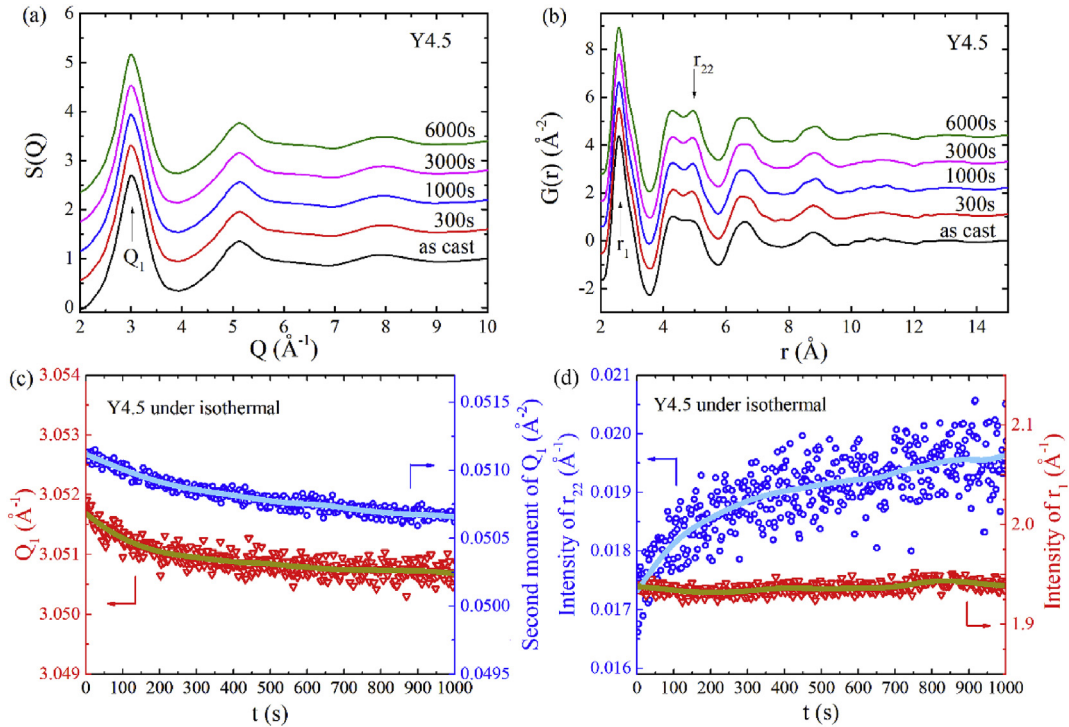


Fig. 7. In-situ synchrotron X-ray diffraction results for Y4.5 alloys under isothermal at T_c . The $S(Q)$ (a) and the $G(r)$ patterns (b) at different isothermal time for Y4.5 alloys. (c) The first moment and the second moment for the FSDP, Q_1 , as a function of time for Y4.5 alloys. The Y-axis range of the plots was set at ± 0.2 – 0.4% . (d) The intensity change of the r_1 and the r_{22} as a function of time for Y4.5 alloys. The Y-axis range of the plots was set at ± 7 – 13% .

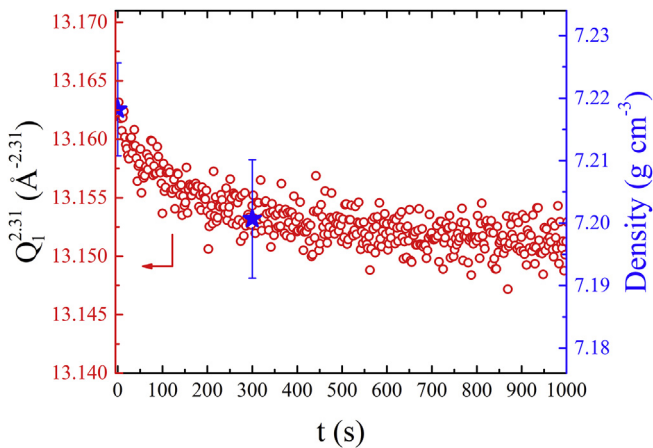


Fig. 8. The change of $Q_1^{2,31}$ as a function of time (left) and measured mass density at the as-cast state and annealed state (right) for Y4.5 alloys. The Y4.5 sample was annealed at T_c for 300s.

there is no chemical phase separation at the nanoscale. The TEM studies have been done by Lee et al. [14] for Y4.5 alloys, suggesting that the phase separation can be excluded due to the small contents of both Nb (4 at%) and Y (4.5 at%). However, the addition of Y element is just 1.5 at% in Y4.5 alloys more than that of Y3 alloys, which results in much pronounced r_{22} peak as shown in Figs. 6 and 7. More interestingly, there is a one-to-one correspondence between the intensity change of the shoulder peak r_{22} and the evolution of the calorimetric anomaly, that is, the AEP, in the supercooled liquid region, further illustrating the role of cluster connectivity on LLPT [9].

4.3. The structure origin of the density change and the nature of a LLPT

The mass density change in a LLPT of MGs is a controversial issue. Some studies showed that the density tends to increase after the LLPT [49]. However, It was argued by the others that density change is not necessary during the LLPT for some cases [50]. Our experimental results show that there is a density change during the LLPT at T_c . The mass density decreases from 7.218 ± 0.007 to $7.201 \pm 0.009 \text{ g cm}^{-3}$ during isothermal annealing. The unusual density decrease may be due to the following possible reasons. First, the Fe-B-based alloys have unique SRO clusters [51], which easily connect to be more ordered at medium-range length scale [8,38]. Second, the Y atom has the largest atomic radius and can play a glue/joint atom role in the medium-range packing scale as illustrated by the PDF results. Fig. 9 is the schematic diagram for the possible packing scheme of the SRO clusters at the medium-range length scale before and after LLPT. Before the LLPT, the SRO clusters show a random packing scheme at the medium-range length scale. The Y atoms locate at some sites which are not energy favored states. After the LLPT, the SRO clusters tend to be more ordered and more connective. Therefore, Y glue/joint atoms can play a role on enhancing the connectivity of the clusters as illustrated by the increasing intensity of r_{22} in Y4.5 alloys after the occurrence of LLPT. However, the local atomic volume somehow could expand when the Y atoms move to energy favored places in the system. Therefore, the density after the LLPT finally decreases and the alloy system after the LLPT tends to be more stable as proved by our experimental results including the calorimetric and density measurements as well as the synchrotron diffraction studies. By consideration of the following evidence, including the structure change, latent heat, and density anomaly, the LLPT in Fe-B-Nb-Y alloys might be a ‘first-order’ type [6,13].

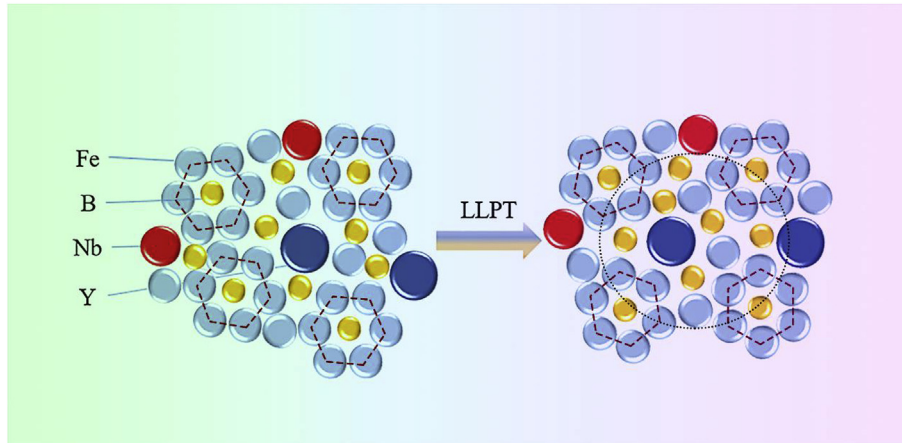


Fig. 9. The schematic diagrams illustrating the evolution of the SRO clusters at a medium-range length scale for Y4.5 alloys under isothermal annealing.

5. Conclusions

In summary, we reveal evidence of the formation of a hidden amorphous phase with configurationally highly-correlated structure in the supercooled liquid region of Fe-B-Nb-Y BMGs of an anomalous exothermic peak using in-situ synchrotron X-ray diffraction measurements. The occurrence of LLPT is associated with an unusual density change. In addition, the new amorphous phase reenters the disordered phase of lower correlation length at a higher temperature during heating. It turns out that the new amorphous phase at T_C stabilizes the supercooled liquid, which might be the structural origin of the good GFA of the Y4.5 alloys. The intensity change of the shoulder peak for the second coordination shell matches well with the AEP in the calorimetric curve, further indicating the important role of cluster connectivity on the amorphous phase transition. The structure change, density anomaly, and the latent heat during the transformation around T_C suggest a possible ‘first-order’ nature of the LLPT in the Fe-B-Nb-Y supercooled liquids.

Acknowledgments

This work was supported by the National Natural Science Foundation of China (Grant No. 51871120, 51501090 and 51571170). SL acknowledges the support by Natural Science Foundation of Jiangsu Province with grant No. BK20171425. XLW acknowledges the support by the Research Grants Council of the Hong Kong Special Administrative Region (CityU Project No. 11216215), and by the National Key R&D Program of the Ministry of Science and Technology (MOST) of China (No. 2016YFA0401501). The synchrotron X-ray work used resources of the Advanced Photon Source, a US Department of Energy (DOE) Office of Science User Facility operated by Argonne National Laboratory under Contract No. DE-AC02-06CH11357.

References

- [1] H.W. Sheng, H.Z. Liu, Y.Q. Cheng, J. Wen, P.L. Lee, W.K. Luo, S.D. Shastri, E. Ma, Polyamorphism in a metallic glass, *Nat. Mater.* 6 (2007) 192–197. <https://doi.org/10.1038/nmat1839>.
- [2] H. Tanaka, General view of a liquid-liquid phase transition, *Phys. Rev. E* 62 (2000) 6968–6976. <https://doi.org/10.1103/PhysRevE.62.6968>.
- [3] H. Tanaka, Relation between thermodynamics and kinetics of glass-forming liquids, *Phys. Rev. Lett.* 90 (2003), 055701. <https://doi.org/10.1103/PhysRevLett.90.055701>.
- [4] J.C. Palmer, F. Martelli, Y. Liu, R. Car, A.Z. Panagiotopoulos, P.G. Debenedetti, Metastable liquid–liquid transition in a molecular model of water, *Nature* 510 (2014) 385. <https://doi.org/10.1038/nature13405>.
- [5] R. Shimizu, M. Kobayashi, H. Tanaka, Evidence of liquid-liquid transition in triphenyl phosphite from time-resolved light scattering experiments, *Phys. Rev. Lett.* 112 (2014), 125702. <https://doi.org/10.1103/PhysRevLett.112.125702>.
- [6] W. Xu, M. Sandor, Y. Yu, H.B. Ke, H.P. Zhang, M.Z. Li, W.H. Wang, L. Liu, Y. Wu, Evidence of liquid-liquid transition in glass-forming La50Al35Ni15 melt above liquidus temperature, *Nat. Commun.* 6 (2015), 7696–7696. <https://doi.org/10.1038/ncomms8696>.
- [7] Y. Katayama, T. Mizutani, W. Utsumi, O. Shimomura, M. Yamakata, K. Funakoshi, A first-order liquid-liquid phase transition in phosphorus, *Nature* 403 (2000) 170–173. <http://www.nature.com/articles/35003143>.
- [8] S. Lan, Y. Ren, X.Y. Wei, B. Wang, E.P. Gilbert, T. Shibayama, S. Watanabe, M. Ohnuma, X. Wang, Hidden amorphous phase and reentrant supercooled liquid in Pd-Ni-P metallic glasses, *Nat. Commun.* 8 (2017) 14679. <https://www.nature.com/articles/ncomms14679>.
- [9] S. Lan, Z. Wu, X. Wei, J. Zhou, Z. Lu, J. Neufeind, X.-L. Wang, Structure origin of a transition of classic-to-avalanche nucleation in Zr-Cu-Al bulk metallic glasses, *Acta Mater.* 149 (2018) 108–118. <https://doi.org/10.1016/j.actamat.2018.02.028>.
- [10] L.E. Tanner, R. Ray, Phase separation in ZrTiBe metallic glasses, *Scripta Metall.* 14 (1980) 657–662. [https://doi.org/10.1016/0036-9748\(80\)90018-6](https://doi.org/10.1016/0036-9748(80)90018-6).
- [11] H. Zheng, Y. Lv, Q. Sun, L. Hu, X. Yang, Y. Yue, Thermodynamic evidence for cluster ordering in Cu₄₆Zr₄₂Al₁₇Y₅ ribbons during glass transition, *Sci. Bull.* 61 (2016) 706–713. <https://doi.org/10.1007/s11434-016-1057-3>.
- [12] S.-B. Qiu, K.-F. Yao, Crystallization kinetics of Zr₄₁Ti₁₄Cu_{12.5}Ni₁₀Be_{22.5} bulk metallic glass in pulsing current pretreatment states, *J. Alloys Compd.* 475 (2009) L5–L8. <http://www.sciencedirect.com/science/article/pii/S0925838808011821>.
- [13] S. Wei, F. Yang, J. Bednarcik, I. Kaban, O. Shuleshova, A. Meyer, R. Busch, Liquid-liquid transition in a strong bulk metallic glass-forming liquid, *Nat. Commun.* 4 (2013) 2083. <https://www.ncbi.nlm.nih.gov/pubmed/23817404>.
- [14] S. Lee, H. Kato, T. Kubota, K. Yubuta, A. Makino, A. Inoue, Excellent thermal stability and bulk glass forming ability of Fe-B-Nb-Y soft magnetic metallic glass, *Mater. Trans.* 49 (2008) 506–512. <https://doi.org/10.2320/matertrans.MBW200732>.
- [15] Q. Zheng, J. Xu, E. Ma, High glass-forming ability correlated with fragility of Mg–Cu(Ag)–Gd alloys, *J. Appl. Phys.* 102 (2007), 113519–113519. <https://doi.org/10.1063/1.2821755>.
- [16] J.H. Na, S.W. Sohn, W.T. Kim, D.H. Kim, Two-step-like anomalous glass transition behavior in Ni–Zr–Nb–Al–Ta metallic glass alloys, *Scripta Mater.* 57 (2007) 225–228. <https://doi.org/10.1016/j.scriptamat.2007.04.014>.
- [17] X.M. Huang, X.D. Wang, Y. He, Q.P. Cao, J.Z. Jiang, Are there two glass transitions in Fe–M–Y–B (M=Mo, W, Nb) bulk metallic glasses? *Scripta Mater.* 60 (2009) 152–155. <https://doi.org/10.1016/j.scriptamat.2008.09.022>.
- [18] S. Lan, M. Blodgett, K.F. Kelton, J.L. Ma, J. Fan, X.L. Wang, Structural crossover in a supercooled metallic liquid and the link to a liquid-to-liquid phase transition, *Appl. Phys. Lett.* 108 (2016) 831–839. <https://doi.org/10.1063/1.4952724>.
- [19] K.F. Kelton, Influence of microalloying on glass formation and crystallization, *J. Alloys Compd.* 434–435 (2007) 115–118. <https://doi.org/10.1016/j.jallcom.2006.08.138>.
- [20] D. Ma, A.D. Stoica, X.L. Wang, Power-law scaling and fractal nature of medium-range order in metallic glasses, *Nat. Mater.* 8 (2009) 30–34. <https://doi.org/10.1038/nmat2340>.
- [21] J. Ding, E. Ma, M. Asta, R.O. Ritchie, Second-nearest-neighbor correlations from connection of atomic packing motifs in metallic glasses and liquids, *Sci. Rep.* 5 (2015) 17429. <https://www.ncbi.nlm.nih.gov/pubmed/26616762>.
- [22] Q. Zeng, Y. Kono, Y. Lin, Z. Zeng, J. Wang, S.V. Sinogeikin, C. Park, Y. Meng, W. Yang, H.K. Mao, W.L. Mao, Universal fractional noncubic power law for

- density of metallic glasses, *Phys. Rev. Lett.* 112 (2014), 185502. <https://www.ncbi.nlm.nih.gov/pubmed/24856706>.
- [23] X. Wu, S. Lan, Z. Wu, X. Wei, Y. Ren, H.Y. Tsang, X. Wang, Multiscale structures of Zr-based binary metallic glasses and the correlation with glass forming ability, *Prog. Nat. Sci. Mater. Int.* 27 (2017) 482–486. <http://doi.org/10.1016/j.pnsc.2017.08.008>.
- [24] J.L. Sutterby, Density by Archimedes' principle using a top loading balance, *J. Chem. Educ.* 53 (1976) 249. <http://pubs.acs.org/doi/abs/10.1021/ed053p249>.
- [25] Y. Huang, W.K. Kin, S. Lan, J.P. Embs, D. Qing, Z. Lu, X.-L. Wang, S.M. Chathoth, Observation of distinct atomic relaxation process in a phase-separated metallic glass-forming melt, *EPL (Europhys. Lett.)* 108 (2014). <http://doi.org/10.1209/0295-5075/108/46001>.
- [26] G. Adam, J.H. Gibbs, On the temperature dependence of cooperative relaxation properties in glass-forming liquids, *J. Chem. Phys.* 43 (1965) 139–146. <https://doi.org/10.1063/1.1696442>.
- [27] D.R. Nelson, Order, frustration, and defects in liquids and glasses, *Phys. Rev. B* 28 (1983) 5515. <https://doi.org/10.1103/PhysRevB.28.5515>.
- [28] G. Tarjus, S.A. Kivelson, Z. Nussinov, P. Viot, The frustration-based approach of supercooled liquids and the glass transition: a review and critical assessment, *J. Phys. Condens. Matter* 17 (2005). <http://iopscience.iop.org/article/10.1088/0953-8984/17/50/R01/meta>.
- [29] H. Tanaka, Two-order-parameter model of the liquid–glass transition. I. Relation between glass transition and crystallization, *J. Non-Cryst. Solids* 351 (2005) 3371–3384. <https://doi.org/10.1016/j.jnoncrysol.2005.09.008>.
- [30] L. Leuzzi, T.M. Nieuwenhuizen, Thermodynamics of the Glassy State, *Condens. Matter Phys-Crc*, 2008.
- [31] R. Soklaski, V. Tran, Z. Nussinov, K.F. Kelton, L. Yang, A locally preferred structure characterises all dynamical regimes of a supercooled liquid, *Philos. Mag.* 96 (2016) 1212–1227. <https://doi.org/10.1080/14786435.2016.1158427>.
- [32] V. Wessels, A. Gangopadhyay, K.K. Sahu, R.W. Hyers, S.M. Canepari, J.R. Rogers, M.J. Kramer, A. Goldman, D. Robinson, J.W. Lee, J.R. Morris, K.F. Kelton, Rapid chemical ordering in supercooled liquid Cu₄₆Zr₅₄, *Phys. Rev. B* 83 (2011). <https://doi.org/10.1103/PhysRevB.83.094116>.
- [33] R. Soklaski, Z. Nussinov, Z. Markow, K. Kelton, L. Yang, Connectivity of the icosahedral network and a dramatically growing static length scale in Cu-Zr binary metallic glasses, *Phys. Rev. B* 87 (2013), 184203. <https://doi.org/10.1103/PhysRevB.87.184203>.
- [34] Y.-C. Hu, Y.-W. Li, Y. Yang, P.-F. Guan, H.-Y. Bai, W.-H. Wang, Configuration correlation governs slow dynamics of supercooled metallic liquids, *Proc. Natl. Acad. Sci. U. S. A.* 115 (2018) 6375–6380. <https://doi.org/10.1073/pnas.1802300115>.
- [35] C. Tang, P. Harrowell, Anomalously slow crystal growth of the glass-forming alloy CuZr, *Nat. Mater.* 12 (2013) 507. <https://doi.org/10.1038/nmat3631>.
- [36] S. Lan, X. Wei, J. Zhou, Z. Lu, X. Wu, M. Feygenon, J. Neufeind, X.-L. Wang, In-situ study of crystallization kinetics in ternary bulk metallic glass alloys with different glass forming abilities, *Appl. Phys. Lett.* 105 (2014), 201906. <https://aip.scitation.org/doi/pdf/10.1063/1.4901905>.
- [37] K.F. Kelton, G.W. Lee, A.K. Gangopadhyay, R.W. Hyers, T.J. Rathz, J.R. Rogers, M.B. Robinson, D.S. Robinson, First X-ray scattering studies on electrostatically levitated metallic liquids: demonstrated influence of local icosahedral order on the nucleation barrier, *Phys. Rev. Lett.* 90 (2003). <http://doi.org/10.1103/PhysRevLett.90.195504>.
- [38] H.W. Sheng, W.K. Luo, F.M. Alamgir, J.M. Bai, E. Ma, Atomic packing and short-to-medium-range order in metallic glasses, *Nature* 439 (2006) 419–425. <https://www.ncbi.nlm.nih.gov/pubmed/16437105>.
- [39] D.B. Miracle, E.A. Lord, S. Ranganathan, Candidate atomic cluster configurations in metallic glass structures, *Mater. Trans.* 47 (2006) 1737–1742.
- [40] P.H. Gaskell, Local and medium range structures in amorphous alloys, *J. Non-Cryst. Solids* 75 (1985) 329–346. <http://www.sciencedirect.com/science/article/pii/002230938590239X>.
- [41] D.B. Miracle, A structural model for metallic glasses, *Nat. Mater.* 3 (2004) 697–702. <https://www.ncbi.nlm.nih.gov/pubmed/15378050>.
- [42] D. Turnbull, Under what conditions can a glass be formed? *Contemp. Phys.* 10 (1969) 473–488. <https://doi.org/10.1080/00107516908204405>.
- [43] Q. Wang, C.T. Liu, Y. Yang, Y.D. Dong, J. Lu, Atomic-scale structural evolution and stability of supercooled liquid of a Zr-based bulk metallic glass, *Phys. Rev. Lett.* 106 (2011), 215505. <https://doi.org/10.1103/PhysRevLett.106.215505>.
- [44] J. Li, H. Men, B. Shen, Soft-ferromagnetic bulk glassy alloys with large magnetostriction and high glassforming ability, *AIP Adv.* 1 (2011), 042110. <http://doi.org/10.1063/1.3654397>.
- [45] T. Paul, A. Loganathan, A. Agarwal, S.P. Harimkar, Kinetics of isochronal crystallization in a Fe-based amorphous alloy, *J. Alloys Compd.* 753 (2018) 679–687. <https://doi.org/10.1016/j.jallcom.2018.04.133>.
- [46] M. Naeem, S. Lan, B. Wang, X.Y. Wei, J. Zhou, Y. Ren, Z.P. Lu, D. Ma, A.D. Stoica, X.L. Wang, Suppression of crystallization in a Ca-based bulk metallic glass by compression, *J. Alloys Compd.* 765 (2018) 595–600. <https://doi.org/10.1016/j.jallcom.2018.06.200>.
- [47] A. Meyer, W. Petry, M. Koza, M.P. Macht, Fast diffusion in ZrTiCuNiBe melts, *Appl. Phys. Lett.* 83 (2003) 3894–3896. <http://doi.org/10.1063/1.1625793>.
- [48] T.A. Waniuk, J. Schroers, W. Johnson, Critical cooling rate and thermal stability of Zr–Ti–Cu–Ni–Be alloys, *Appl. Phys. Lett.* 78 (2001) 1213–1215. <https://doi.org/10.1063/1.1350624>.
- [49] J.J.Z. Li, W.K. Rhim, C.P. Kim, K. Samwer, W.L. Johnson, Evidence for a liquid–liquid phase transition in metallic fluids observed by electrostatic levitation, *Acta Mater.* 59 (2011) 2166–2171. <https://doi.org/10.1016/j.actamat.2010.12.017>.
- [50] R. Busch, I. Gallino, Kinetics, thermodynamics, and structure of bulk metallic glass forming liquids, *JOM* 69 (2017) 2178–2186. <http://doi.org/10.1007/s11837-017-2574-5>.
- [51] H. Tian, C. Zhang, J. Zhao, C. Dong, B. Wen, Q. Wang, First-principle study of the structural, electronic, and magnetic properties of amorphous Fe–B alloys, *Phys. B Condens. Matter* 407 (2012) 250–257. <http://doi.org/10.1016/j.physb.2011.10.042>.